Journal of Materials Chemistry B

ROYAL SOCIETY OF CHEMISTRY

COMMUNICATION

View Article Online
View Journal | View Issue

Cite this: J. Mater. Chem. B, 2025, 13, 6329

Received 10th February 2025,
Accepted 30th April 2025

DOI: 10.1039/d5tb00302d

rsc.li/materials-b

Engineered $Ti_3C_2(O,Cl)$ MXenes with dual functionalization: a new Frontier in targeted head and neck squamous cell carcinoma and breast adenocarcinoma†

Jhansi Chintakindi, ‡[a] Ganesh Panditrao Lahane,‡[b] Arti Dhar*[b] and Afkham Mir *[a]

$Ti_3C_2T_x$ MXenes have attracted significant attention in the realm of anticancer therapeutics owing to their remarkable properties, including cyto-compatibility and targeted drug delivery capabilities. In this study, Ti_3C_2 was intentionally modified with both chlorine and oxygen surface groups, as each of these functional groups have individually demonstrated promising anticancer properties. Our aim was to combine them in a single compound to explore how this dual-functionalized material might perform in a therapeutic context. This study synthesizes $Ti_3C_2(O,Cl)$ MXenes using a novel electrochemical etching technique that allows for precise tailoring of the surface terminations with O and Cl groups. The synthesised $Ti_3C_2(O,Cl)$ has biological activity in two cancerous (FaDu and MCF-7) and two normal (H9C2 and HEK-293) cell lines. The results of cytotoxicity data showed that the observed toxic effects were higher against cancerous cells (~91%) than normal cells (~40%). The mechanisms of potential toxicity were also elucidated. The synthesized $Ti_3C_2(O,Cl)$ MXene has an effect on oxidative stress, resulting in an increase of more than 91.44% in reactive oxygen species (ROS) production in malignant cells. The results of this study provide major insights to date into the biological activity of $Ti_3C_2(O,Cl)$ MXenes and develop their application in anticancer treatments.

1. Introduction

Cancer (karkinos) has a profound and far-reaching impact on human life, affecting individuals, families, and society worldwide. Countless chronic novel instances of cancer are discovered each year, and the disease affects millions of lives globally, resulting in a significant cause of illness and mortality. With 8.97 million deaths annually, cancer is currently the second leading cause of death worldwide.[1] It is projected to overtake all other causes of death by 2060 (about 18.63 million deaths annually).[2] Multiple methodologies are available for the management of carcinoma, including interventions such as chemotherapy, radiotherapy, immunotherapy, hormone therapy, and targeted medication therapy.[3] Nonetheless, each technique has limitations and detrimental effects. Therefore, it is essential to identify a reliable and effective method that can prolong life expectancy while improving health. A versatile framework of biocompatible and biodegradable systems is made possible by nanomedicine, which can be employed to deliver typical chemotherapeutic drugs *in vivo*, boost their bioavailability and concentration amid tumor tissue, and improve their release profile. Among them, a few nanoparticles including gold nanoparticles,[4] molybdenum oxide (MoO_x),[5] silver nanoparticles,[6] copper selenide (CuSe),[7] tungsten disulfide (WS_2),[8] self-assembled organic polyamic materials,[9] dyes,[10] *etc.* have demonstrated excellent cytotoxicity towards cancer cell lines.

In recent years, MXenes, a family of two-dimensional (2D) nanomaterials that were discovered in 2011, have attracted significant attention due to their intriguing anticancer properties. MXenes possess numerous functional groups that enable them to facilitate drug transport, ensuring targeted delivery with increased toxicity towards cancer cells while being cytocompatible.[11] MXenes are synthesised by etching the weakly bonded A-group elements from bulk ternary carbides/nitrides of MAX phases. It has a general formula of $M_{n+1}X_nT_x$, where M is an early transition metal (such as Sc, Ti, Zr, Hf, Zr, *etc.*), A is a group (12–16) element of the periodic table, X represents carbon and/or nitrogen, T_x represents surface terminations (such as –F, –Cl, –OH, –O, *etc.*) and n = 1–3.[12–14] MXene production originated in 2011 using hydrofluoric acid (HF) as its principal etchant.[15] It was in 2015 that it transitioned into a 2D material category. Several alternative methods of synthesis have been developed to address the potential hazards associated with using HF. The methods used include *in situ* HF etching,[16] molten salt

[a] Department of Chemical Engineering, BITS Pilani, Hyderabad Campus, Telangana, India. E-mail: mirafkham@hyderabad.bits-pilani.ac.in
[b] Department of Pharmacy, BITS Pilani, Hyderabad Campus, Telangana, India. E-mail: arthidhar@hyderabad.bits-pilani.ac.in

† Electronic supplementary information (ESI) available. See DOI: https://doi.org/10.1039/d5tb00302d

‡ The authors contributed equally to this work.

methods,[17] alkali-based procedures,[18] minimally intensive layer delamination (MILD),[19] hydrothermal techniques,[20] ball milling approaches[21] and electrochemical etching.[22] However, there exist several limitations associated with the alternative synthesis processes, such as the extended etching times and the limited efficiency in tuning the functional groups of the synthesised $Ti_3C_2T_x$. These challenges underscore the significance of safer, more effective, and regulated etching strategies in the synthesis of $Ti_3C_2T_x$ MXenes. It is worth mentioning that electrochemical etching has gained attention as a safer, simpler, and more dependable alternative to HF-based techniques for the generation of $Ti_3C_2T_x$ MXenes, offering the potential to produce large quantities of high-quality materials and tune the functional groups. The electrochemical method has emerged as a fluoride free, environmentally sustainable method for the synthesis of MXenes with highly tunable and biocompatible surface terminations (–O, –Cl, and –OH).

The electrochemical etching framework utilizes an electric current that helps the ions to move from the electrolyte into the bulk materials, thus weakening the van der Waals forces that bind the bulk layers together. The etching process effectiveness is greatly influenced by the combination of electrolyte composition, operating voltage, and precursor selection.[23] By altering electrochemical factors like current, voltage, and the electrolyte, it is possible to precisely control the MXene surface terminations. This approach provides a precise method for expelling challenging 'A-phase' materials with minimal etching time. It also offers the ability to control functionalization options such as –O, –OH, –Cl, or –F.

Firstly, we synthesised Ti_2CT_x utilizing a milder electrolyte and lower potentials such as HCl at +0.6 V to etch the A layer from the MAX phase.[23] Researchers found that the MXenes underwent complete conversion into carbon derived carbon (CDC) after being etched for 5 days. During the process, they also observed white layer depositions on the platinum counter electrode and that the surface terminations attached to Ti_2C are –O, –C, and –Cl. Another study conducted electrochemical etching of $Ti_3C_2T_x$ MXenes utilizing a binary aqueous electrolyte (NH_4Cl + TMAOH) at a pH greater than 9.[24] In the study, etching was carried out at higher potentials of approximately +5 V. It was found that the prepared samples are terminated with –OH as T_x, and the overall etching yield was initially low at around 40%. However, after implementing recycling methods, the yield was increased to 60%. Furthermore, scientists utilized a mixture of LiCl and KCl as etchants through a molten salt procedure to prepare the initial MAX Ti_2AlC phase.[25] They then employed a one pot *in situ* E-etching method at 1.3 V for extended periods of 24 hours, conducted at a high temperature of 500 °C. They found that Ti_2CT_x have surface terminations with –Cl, but after washing with ammonium persulfate, the T_x changed to the –O functional group.[25] While electrochemical etching techniques have been employed to synthesize Ti_3C_2, these methods have produced functional groups without precise tuning.

In anticancer applications, the generation of reactive oxygen species (ROS) relies on the idea that increasing ROS levels above a lethal threshold selectively eliminates cancer cells. The –O functional groups attached to Ti_3C_2 MXenes act as carriers for drug delivery, enhancing ROS production towards cancer cells. Additionally, the chlorinated compounds attached to Ti_3C_2 MXenes exhibit a cytotoxic effect, suggesting resilient anticancer activity. A recent study tested the bioavailability of $Ti_3C_2T_x$ on two normal (MRC-5 and HaCaT) and two cancerous (A549 and A375) cell lines.[26] It was observed that the prepared Ti_3C_2 MXenes had surface terminations such as –OH, =O, and C=O–OH groups, showing higher cytotoxic effects against cancerous cells compared to normal ones. Additionally, the study noted that MXene suspensions were non-toxic only in HaCaT cells, with cell viability remaining above 70% and the lowest levels of ROS production. In contrast, the highest ROS levels (approximately 89%) were observed in A375 cells.

In 2020, researchers further tuned Ti_3C_2 into Ti_3O_2 and assessed the cytotoxicity *in vitro* against human epithelial breast (MCF-10A), breast cancer (MCF7), human immortalized keratinocytes (HaCaT), and human malignant melanoma (A375) cell lines.[27] They synthesized three types of MXene samples: (a) Ti_3C_2, (b) sonicated Ti_3C_2, and (c) thermally oxidized Ti_3C_2, mostly with –O and –OH terminations. The results showed that all three MXene samples were toxic towards the cell lines, with greater toxicity towards melanoma cells. The toxicity of all three increased with the concentration of MXenes. At a concentration of 125 mg L^{-1}, the sonicated and oxidized MXenes were lethal to A375 cells while being relatively less toxic to HaCaT cells. In 2020, another study reported the effect of Chlorin e6 (Ce6) (family of chlorine group) on photodynamic delivery for cancer cell killing and intracellular drug delivery.[28] In this study, chlorin e6 was fabricated with gas vesicles (GVs) to study the cytotoxicity of cancerous cells such as a human hypopharyngeal cancer cell line (FaDu-GFP) and the MCF-7 cell line. Ce6 molecules are excited by light from singlets to triplet states improving the energy transfer of O_2 to generate singlet oxygen, which causes oxidative damage leading to cell death. Ce6-GV when compared with free Ce6-based nanoparticles was 200-fold more effective. Furthermore, the cytotoxic effect of chlorine dioxide (an effective disinfectant of chlorine) was studied on small-cell lung cancer (SCLC) cells and human umbilical vein endothelial cells (HUVECs).[29] The study reported that apoptotic cell death ranged from 37% to 49% for the DMS114 cell line, while in the HUVEC control it ranged from 19% to 25%.

Ti_3C_2 synthesised through various routes has been explored as a potential anticancer agent.[30] However, these studies did not prioritize optimization of ROS promoting functional groups on Ti_3C_2 which are vital for maximising anticancer properties. In some cases, Ti_3C_2 has been combined with photothermal methods to improve its therapeutic efficiency.[31,32] The high surface area of Ti_3C_2 has also been leveraged by using its carrier for drug delivery, including encapsulation of doxorubicin,[31] which is widely used as a chemotherapeutic agent.

In this work, the $Ti_3C_2T_x$ MXenes are electrochemically etched using chronoamperometry techniques or preliminarily intercalated at −0.6 V followed by etching at a potential of

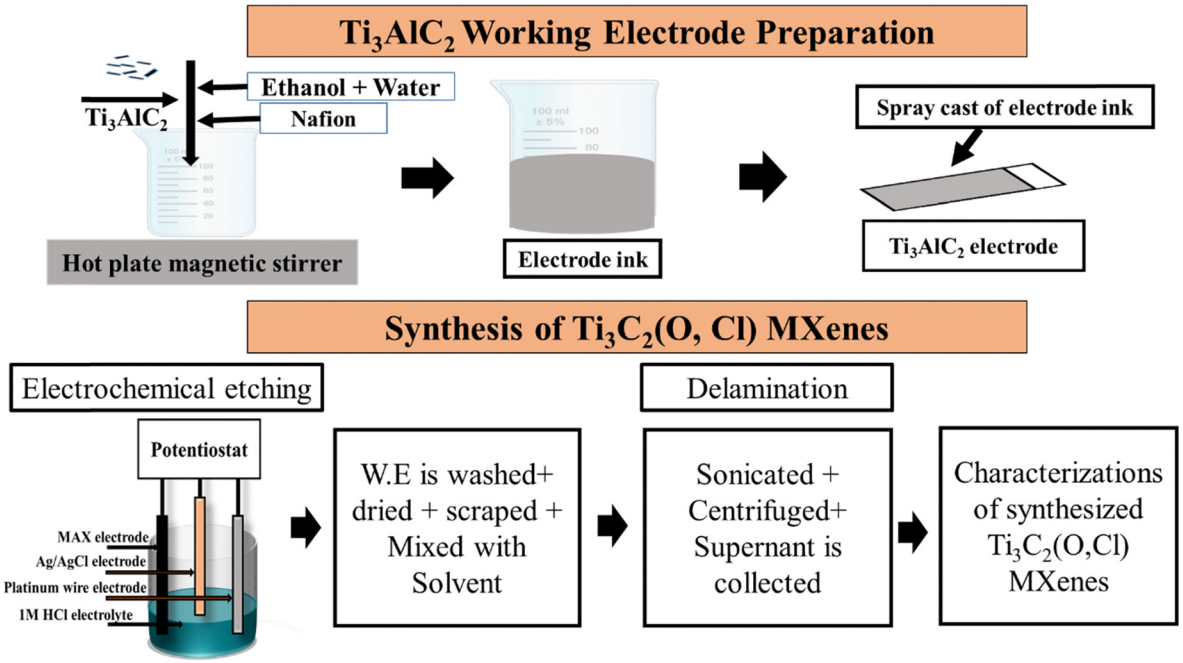

Fig. 1 Schematic diagram of electrochemical synthesis of $Ti_3C_2T_x$ MXenes from Ti_3AlC_2 pristine powder.

+0.6 V to produce Ti_3C_2O and Ti_3C_2Cl. The synthesis process of the Ti_3C_2(Cl,O) MXenes, as outlined in the ESI,† S1, is illustrated schematically in Fig. 1. Subsequently, the prepared MXenes were subjected to characterization. The produced MXenes were subjected to *in vitro* analysis as detailed in the ESI,† S2. The prepared MXenes exhibit attributes for *in vitro* cytotoxicity against cancerous and normal cells. Our research also elucidates oxidative stress phenomena as the potential mechanisms of toxicity. The findings of this study offer crucial insights into the toxicity of Ti_3C_2O and Ti_3C_2Cl in relation to both normal and cancerous cell lines. However, the lack of this information has been a significant barrier to advancing research and development in drug delivery systems for anti-cancer therapies involving MXenes.

2. Materials and methods

2.1 Materials used for the preparation of $Ti_3C_2T_x$ MXenes

Ti_3AlC_2 MAX powder was purchased from Nanochemazone, Aritech (India), ethanol was purchased from analytical CS reagent (India), de-ionized water and Nafion binder were purchased from Sigma Aldrich (India), HCl was purchased from Finer (India), and dimethyl sulfoxide (DMSO) was purchased from SRL (India).

2.2 Materials used for anticancer studies

FaDu, MCF-7, HEK-293, and H9C2 cells were purchased from National Center for Cell Science (Pune, India). RPMI-1640 (AL162A), DMEM (AL219A), trypsin (TCL007), and MTT (TC191) were purchased from Himedia (Himedia Laboratories Pvt Ltd, Mumbai, India). FBS (10270-106) was purchased from Gibco (Gibco, Life technology, E.U, South American). Doxorubicin (D1515) and 2′,7′-dichlorofluorescin diacetate (D6883) were purchased from Sigma-Aldrich (Sigma-Aldrich, St. Louis, USA).

2.3 Material characterization used for $Ti_3C_2T_x$ MXenes

Powdered X-ray diffraction (PXRD) (Rigaku Ultima-IV, Ultima) (X-ray source – copper, scan rate – 1° min^{-1} to 5° min^{-1}, 2θ range – 5–90°), X-ray photoelectron spectroscopy (XPS) (Thermo Fisher Scientific Pvt. Ltd UK) (source – aluminium K-alpha, kinetic energy – 5 to 1500 eV), FE-SEM (FEI, Apreo Lovac) (source – copper, magnification – 10× to 30 000×, resolution – up to 2 nm), confocal Raman spectrometry (Lab Ram HR Horiba) (range – 300 to 2500 cm^{-1}), high-resolution transmission electron microscopy (HR-TEM) (Jeol Jem 2100 plus, India) (resolution – 1 nm), and a potentiostat/galvanostat (Metro-Ohm, India) (range −10 to +10 V) were used for material characterisation.

2.4 Statistical methods

Statistical analyses were performed using Graph Pad prism 9 software. One-way ANOVA followed by the Bonferroni *post hoc* test was used to define statistical significance. $p < 0.05$ was considered statistically significant.

3 Results and discussion

3.1 Synthesis and characterization of Ti_3C_2 (O,Cl)

In order to ascertain the redox potentials of both the working electrode (Ti_3AlC_2) and the electrolyte, initial cyclic voltammetry was carried out with a potential range of −1.5 V to +1.5 V, as shown in Fig. 2(A). The redox potentials of −1.19 V, −1.32, and −0.44 V were observed in the CV curve and also

exhibited a linear increase in current from 0 to +1.5 V, followed by a small peak at −0.4 V during the forward scan and a peak at −1.1 V during the backward scan. The counter electrode used was platinum (Pt), while the Ag/AgCl electrode served as the reference.

1.23 V indicates reduction processes associated with water splitting, and −0.44 V indicates the reduction of titanium species, so the potential values of −0.6 V for intercalation and +0.6 V for etching were selected for the present study. Specifically, −0.6 V was sufficiently negative to facilitate efficient H^+ ion intercalation while minimizing significant side reactions, such as water reduction or the disruption of Ti–C bond stability. Conversely, the application of +0.6 V was favourable for effectively etching aluminium from the Ti_3AlC_2 MAX phase without compromising the structural integrity of the resulting $Ti_3C_2T_x$ MXenes. The synthesis of $Ti_3C_2T_x$ MXenes involves the application of chronoamperometry, where a potential of −0.6 V was applied for 5 seconds to introduce an ion into the Ti_3AlC_2 compound. This was followed by applying a potential of +0.6 V for 5 seconds to remove the Al ions from the Ti_3AlC_2 MAX compound, as shown in Fig. 2(B). Then, the electrochemical etching process was carried out for a total duration of 6000 s, as depicted in Fig. 2(C), resulting in the production of Ti_3C_2 (O,Cl) MXenes. We subsequently performed delamination on the resultant MXenes to isolate the unetched Ti_3AlC_2 and $Ti_3C_2T_x$ MXenes.

After synthesis, the Ti_3C_2 MXene was washed, sonicated, and centrifuged and the delaminated material was further characterised. XRD analysis of the synthesised Ti_3C_2 MXene is shown in Fig. 2(D); major peaks of (002), (004), (101), (103), (104), (105), (107), (108), and (109) in the diffraction pattern in the 2 theta range from 5° to 75° are consistent with the previously reported Ti_3C_2 MXene.[33] It was observed that the majority of diffraction peaks' intensity decreased from the pristine sample to $Ti_3C_2T_x$ samples, and also characteristic (*i.e.* 104) peaks and several broad and low-intensity peaks in the 2 theta range from 5° to 75° were observed; these characteristics indicate the successful reduction of Ti_3AlC_2 to layers of Ti_3C_2 MXene.[34] The shift of the (002) peak observed from 10.627° to 10.36° (±0.02°) suggests that the interlayer distance has increased. The characteristic peaks at 39.86° (104) and 42.83° (105) corresponding to Ti_3AlC_2 show reduced intensities, indicating partial etching of Al layers and successful MXene formation *via* the electrochemical technique. This reduction in intensity indicates that a substantial portion of the Ti_3AlC_2 parent material has undergone successful conversion into $Ti_3C_2T_x$ MXene. The weight percentage of $Ti_3C_2T_x$ formed through electrochemical etching was 73.7%[34,35] which was calculated through formula weight percentage = $1 - 0.2x + 0.013x^2$, where x is the ratio of intensity of the 39.86° peak to the intensity of the 10.36° peak.[36] Hence, XRD confirms the successful etching of Ti_3AlC_2 to form Ti_3C_2(O,Cl) MXene, evidenced by the shift in the (002) peak and reduced intensity of the Ti_3AlC_2 (104) peak. The increased interlayer spacing indicates the incorporation of surface terminations and partial removal of aluminium.

The $Ti_3C_2T_x$ MXenes were subjected to further characterization *via* SEM to validate the alterations in the structure and morphology, as depicted in Fig. 3(A) and (B) for the pristine Ti_3AlC_2 and synthesized $Ti_3C_2T_x$ MXenes. The observed morphology aligns closely with the existing literature, exhibiting a

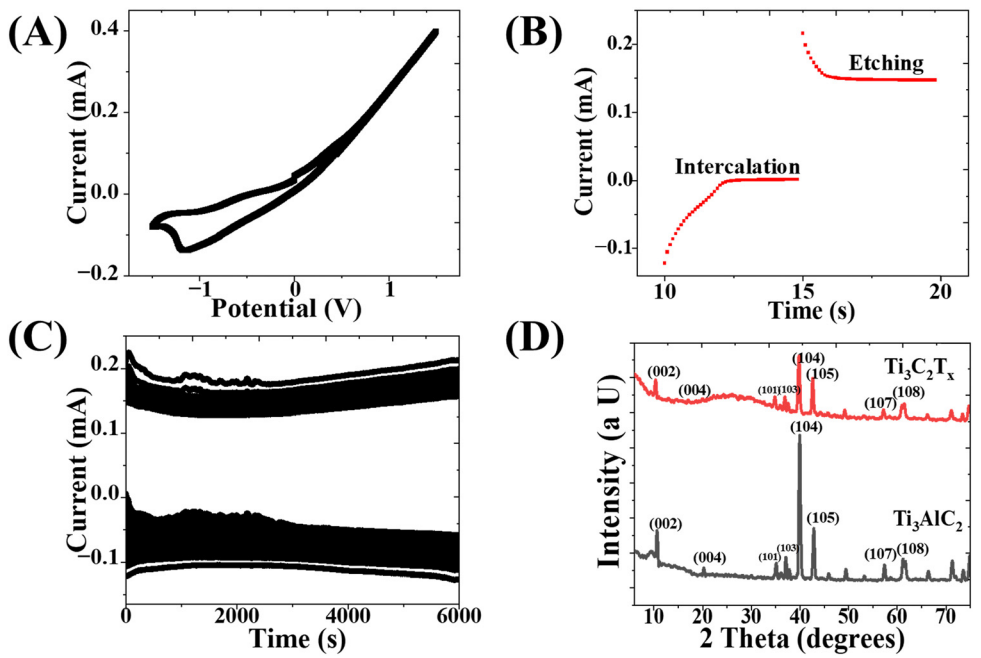

Fig. 2 (A) Cyclic voltammetry curve for the Ti_3AlC_2 MAX electrode at a potential window of −1.5 V to +1.5 V, (B) a representation of the chronoamperometry curve for 5 s each at potentials of −0.6 V (intercalation) and +0.6 V (etching), (C) chronoamperometry including both intercalation and etching for 6000 s and (D) XRD analysis for the pristine Ti_3AlC_2 Max phase and $Ti_3C_2T_x$ MXene.

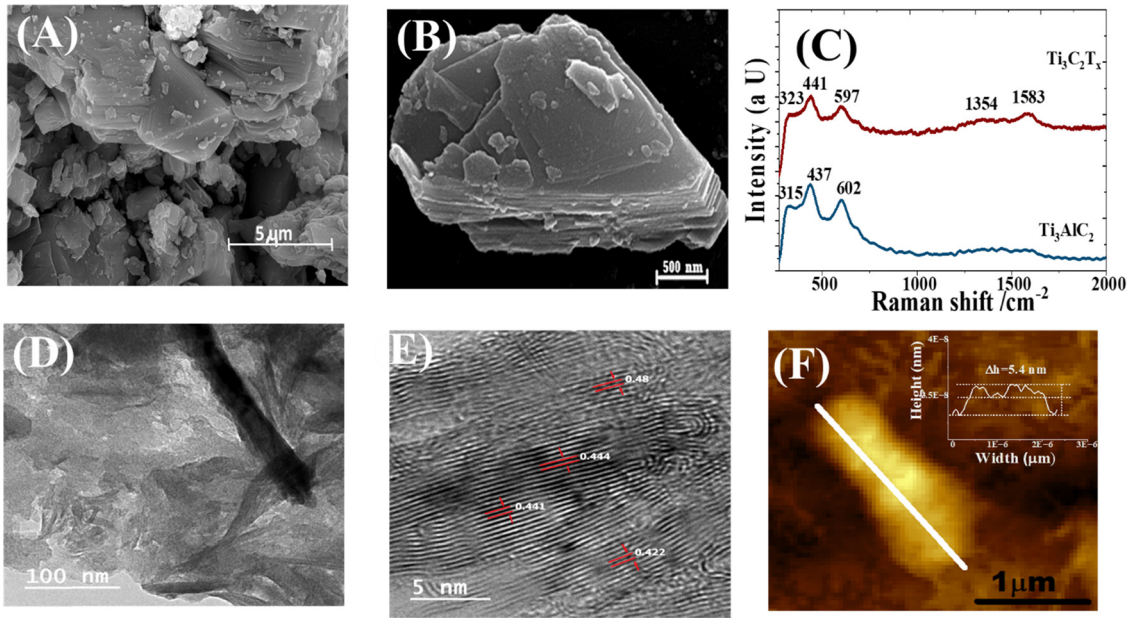

Fig. 3 SEM images for (A) the pristine Ti_3AlC_2 MAX phase and (B) Ti_3C_2(O,Cl) MXene; (C) Raman analysis for Ti_3AlC_2 and Ti_3C_2(O,Cl); (D) TEM images for Ti_3C_2(O,Cl) MXene at 100 nm; (E) TEM image of Ti_3C_2(O,Cl) at 5 nm and (F) AFM image of Ti_3C_2(O,Cl) with a height of 5.4 nm.

microstructure reminiscent of an accordion. The disparity in surface features between unetched Ti_3AlC_2 and $Ti_3C_2T_x$ was remarkably pronounced. While the former presents a polished surface, the latter experiences delamination and results in a coarser surface when a minimal potential was applied. The morphological transformation serves as a compelling indicator of the efficacy of the electrochemical etching technique.

Furthermore, the Raman analysis of the synthesized $Ti_3C_2T_x$ MXenes, illustrated in Fig. 3(C), showed significant peaks at 312 cm^{-1}, 435 cm^{-1}, and 605 cm^{-1} for the Ti_3AlC_2 MAX sample. Conversely, the $Ti_3C_2T_x$ sample displayed peaks at 323 cm^{-1}, 431 cm^{-1}, 597 cm^{-1}, and 1583 cm^{-1}. The noted transition in the peak from 312 to 323 cm^{-1} signifies the replacement of the 'Al' element in Ti_3AlC_2 MAX with surface terminal groups. The peak at 323 cm^{-1} corresponds to the vibrational modes of the oxygen atoms.[37] The spectral region located at 435 cm^{-1} is indicative of in-plane (E_g) vibrations of surface groups that are attached to titanium atoms.[38] The region around 597 cm^{-1} can be attributed to the E_g vibrations of carbon atoms in the $Ti_3C_2T_x$ MXene, which possesses terminal hydroxyl (–OH) groups and represents Ti_3C_2(OH).[39] Furthermore, the peak at 1548 cm^{-1} corresponds to the G bands of carbon groups. The Raman examination revealed the presence of Ti–C, Ti–Cl, and Ti–O bonds in the produced $Ti_3C_2T_x$ MXenes. The surface terminations consisted of Cl^-, O^- and OH^- groups, resulting in the formation of Ti_3C_2Cl, Ti_3C_2O and Ti_3C_2(OH) species.

The detailed structural alterations in the $Ti_3C_2T_x$ sample are further revealed by low magnitude high resolution transmission electron microscopy (HRTEM). Fig. 3(D) and (E) show the HRTEM image with high crystallinity of the Ti_3C_2(O,Cl) MXenes. Further analysis of Ti_3C_2(O,Cl) shows an interlayer spacing of ~0.4 nm representing the (004) plane.[40] Thus, the demonstrated increase in the interlayer gap enhances the interfacial charge transfer and electrolytic ion accessibility to electroactive regions. Additionally, the TEM results align with the XRD findings. The height profile obtained from the atomic force microscopy (AFM) measurement indicates that the thickness of the Ti_3C_2(O,Cl) MXene flakes was 5.4 nm as shown in Fig. 3F. This value was in agreement with the reports that have been made in the past on few-layer flakes.

Further investigation was carried out on the synthesized MXenes utilizing X-ray photoelectron spectroscopy (XPS) analysis, as illustrated in Fig. 4(A to E). The investigation into the formation of surface terminations (T_x) on Ti_3C_2 MXenes encompassed elemental analyses of titanium, carbon, aluminium, chlorine, and oxygen. The XPS spectra for the Ti peak, as depicted in Fig. 4(A), show Ti-2p bonds with spin orbitals of $2p_{1/2}$ and $2p_{2/3}$. In the analysis of the Ti peak, Ti–C bonds appear at 455.03 eV and 461.20 eV (with ΔB.E of ~6.17), Ti–O bonds at 459.12 eV and 464.96 eV (with ΔB.E of ~5.7) and Ti–Cl bonds at 460.06 eV. Thus, the Ti peak indicates bonding with C, Cl, and O, forming Ti–C, Ti–Cl, and Ti–O bonds. Furthermore, it was observed that the Ti peak has no bond formation with Al (*i.e.* no Ti–Al bond), which confirms the successful etching of Al from the sample surface. From the Ti peaks, the ratio of Ti–Cl/Ti–C was found to be 0.57 and the ratio of Ti–O/Ti–C was 2.9 as shown in Table 1, and thus the –O surface terminations are more compared to –Cl terminations as T_x on $Ti_3C_2T_x$.

To further investigate the absence of Al in the prepared sample, the Al-2p peak was fitted as shown in Fig. 5(B). It was observed that Al oxides emerged at 75 eV, forming an Al–O bond, which confirms the removal of Al from the sample surface, resulting in the formation of Ti_3C_2(O,Cl). In addition to the Ti peak and Al peak, we have also investigated the Cl

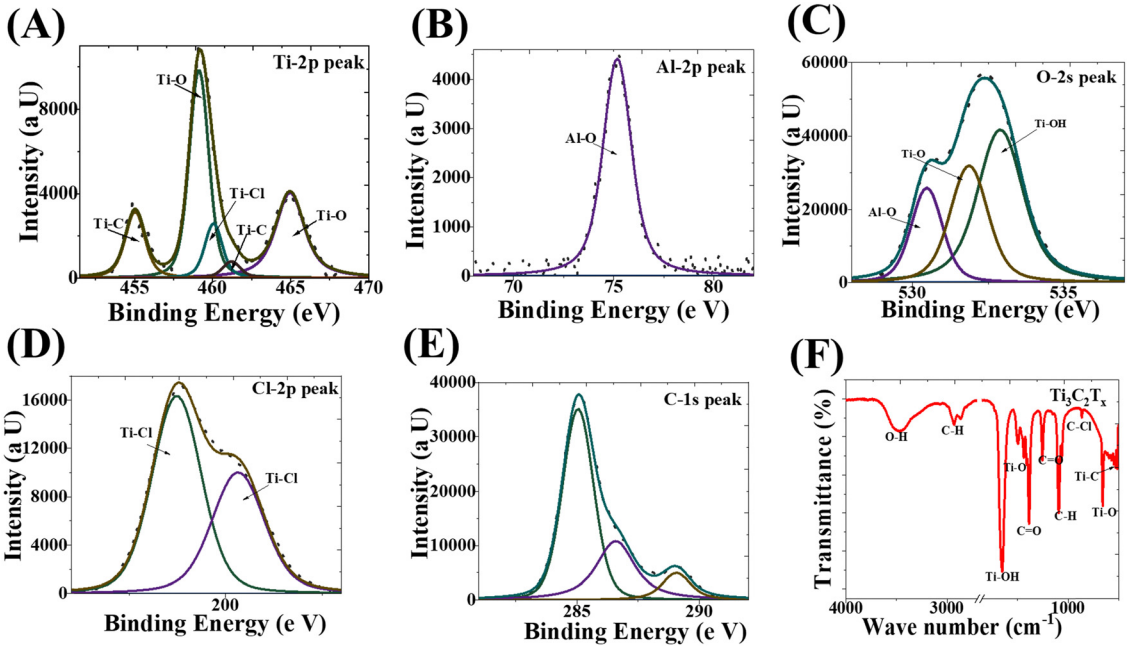

Fig. 4 XPS analysis of $Ti_3C_2(O,Cl)$ MXene for (A) Ti peak fitting, (B) Al peak fitting, (C) Cl peak fitting, (D) O peak fitting and (E) C peak fitting and (F) FTIR analysis for $Ti_3C_2(O,Cl)$ MXene.

Table 1 Toxicity of $Ti_3C_2T_x$ MXenes on different cell lines

Ref.	Cancer cell	Normal cells	ROS (MFI/%)	Cell viability (%)	Effect of –O and –Cl	Dose in mg L^{-1} (incubation time)	Effects
26		HaCaT	29	70	—	50–500 (24 h)	No toxicity
		MRC-5	—	—			
	A549						
	A375		89	>70			Highest ROS
27	MCF7			>70	–O: high anticancer activity	62.5–500 (24 h)	Toxicity increases with the Ti_3C_2 concentration
	A375			>70			
		HaCaT		>70	—		
		MCF-10A		>70	—		
28	FaDu-GFP	—	500 MFI	~ <5	–Cl: some anticancer activity	24 h with light exposure	DCF fluorescence recorded using a plate reader. Mean fluorescence is intensity not reported.
	MCF-7	—	400 MFI	~ <10			
29		HUVEC	—	>75	–Cl: moderate anticancer activity	1–5 (48 h) 0.1–10 (48 h)	Cl has potential for anticancer activity and is less toxic for normal cells. Apoptosis by FACS
	SCLC	—	—	<54			
Present work		H9C2		>65	Synergistic effect of Cl and O gives a high anticancer effect	6.25–500 (24 h)	Less toxic than Doxo for normal cell lines
		HEK-293	>16	>65			
	FaDu		>91	<30			
	MCF7	—	—	>70			More toxic to FaDu and MCF-7

peaks, O peaks, and C peaks, as shown in Fig. 4(C), (D) and (E), respectively, to acquire a greater comprehension regarding the formation of surface termination groups. Likewise, from the peak of O-2s illustrated in Fig. 4(C), it is evident that –O appears as Ti–O, Ti–OH and Al–O at 530.74 eV, 531.86 eV, and 532.89 eV, respectively. From the O peak, it was observed that the ratio of Ti–O/Ti–OH was 0.657, indicating that Ti–OH predominates over the Ti–O bond as represented in Table 2. From the Cl-1s peak illustrated in Fig. 4(D), Cl-2p establishes bonds with Ti as Ti–Cl at 198.73 eV and 200.32 eV (with ΔB.E of approximately 1.6). The XPS analysis indicates that Al has been removed from the surface of the sample, resulting in the formation of surface terminations such as –Cl, –OH, and –O. Consequently, a higher level of –O and –Cl surface terminations as T_x bonded to $Ti_3C_2T_x$ significantly enhances the properties that contribute to the efficacy of anti-cancer activity.

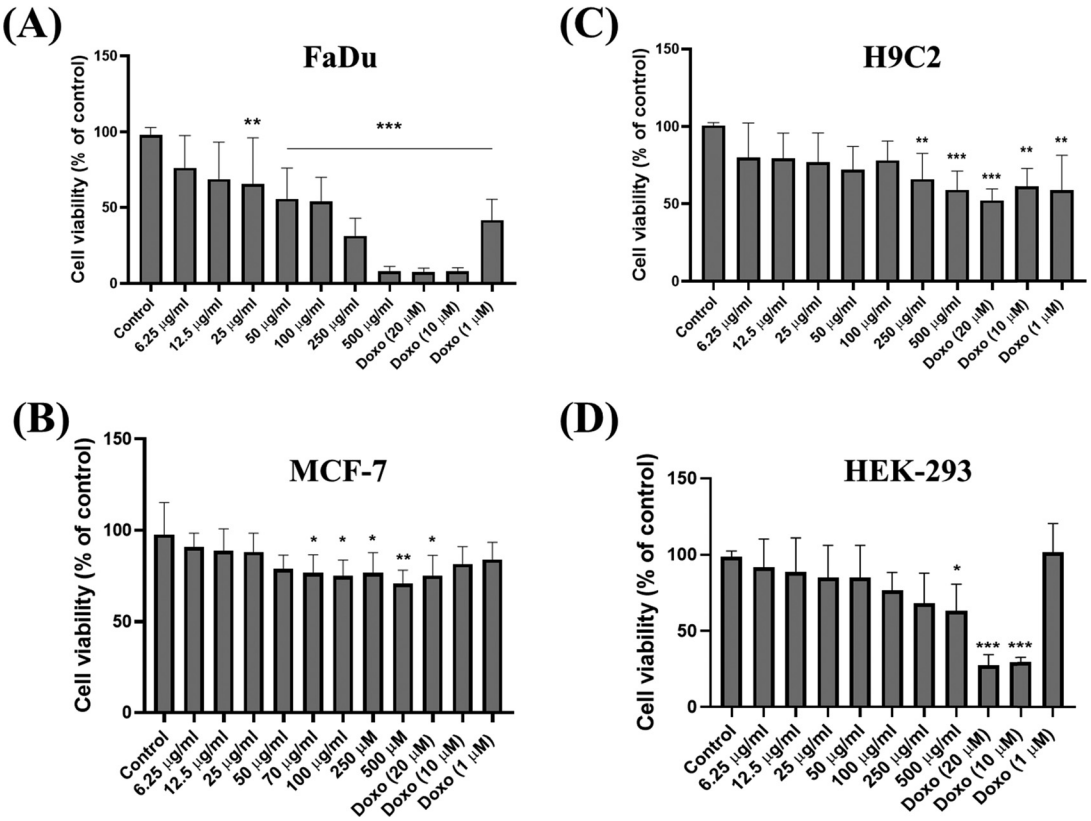

Fig. 5 Cytotoxic effect of MXene on FaDu, MCF-7, H9C2, and HEK-293 cells (A, B, C, and D, respectively) for a time duration of 24 h. Data are shown as mean ± SD (n = 3) of three independent experiments. *** $p < 0.001$, ** $p < 0.01$, and * $p < 0.05$ *vs.* respective control.

Table 2 XPS analysis for the Ti peak and the O peak

Ti peak					
Compound	$2p_{3/2}$ (eV)	$2p_{1/2}$ (eV)	FWHM	ΔB.E (eV)	Ratio
Ti–C	455.03	461.20	2.09 and 2.2	6.17	$\frac{Ti-Cl}{Ti-C}=0.57$
Ti–O	459.59	464.86	2.3 and 2.2	5.7	$\frac{Ti-O}{Ti-C}=2.97$

O peak		
Compound	2s (eV)	Ratio
Ti–O	531.01	$\frac{Ti-O}{Ti-OH}=0.65$
Ti–OH	532.84	

Furthermore, Fourier transform infrared spectroscopy (FTIR), as shown in Fig. 4(F), was used to analyse the functional groups on the surface of $Ti_3C_2T_x$. The peaks observed at 3471 cm^{-1}, 2860–2932 cm^{-1}, 1650 cm^{-1}, 1495 cm^{-1}, 1222–1387 cm^{-1}, 1093 cm^{-1}, 863 cm^{-1} and 658 cm^{-1} correspond to the stretching vibrations of O–H, C–H, Ti–OH, Ti–O, C═O, C–H, C–Cl, and Ti–O, respectively, which were in accordance with the findings of prior investigations from XPS and Raman analyses.

3.2 Results of the *in vitro* cytotoxicity assay

The biological activity of the Ti_3C_2(O,Cl) MXene on two normal (H9C2 and HEK-293) and two cancerous (FaDu and MCF-7) cell lines were determined. The results concerning cell viability, obtained using an MTT assay for 24 h and 48 h, are shown in Fig. 5(A)–(D) and 6(A) and (B). The viability of the cells decreased significantly with increasing concentration of Ti_3C_2(O,Cl) MXene for time points of 24 and 48 h ($p < 0.001$). The cytotoxicity of the tested Ti_3C_2(O,Cl) MXene material was strongly dependent on the cell line. The highest cytotoxicity was observed in the FaDu cell line followed by MCF-7 as shown in Fig. 5(A) and (B) for 24 h. However, in H9C2, Doxo 20 μM showed more cytotoxicity compared to Ti_3C_2(O,Cl) MXene, Fig. 5(C). Notably, Ti_3C_2(O,Cl) MXene exhibited significantly lower cytotoxic effects on H9C2 and HEK-293

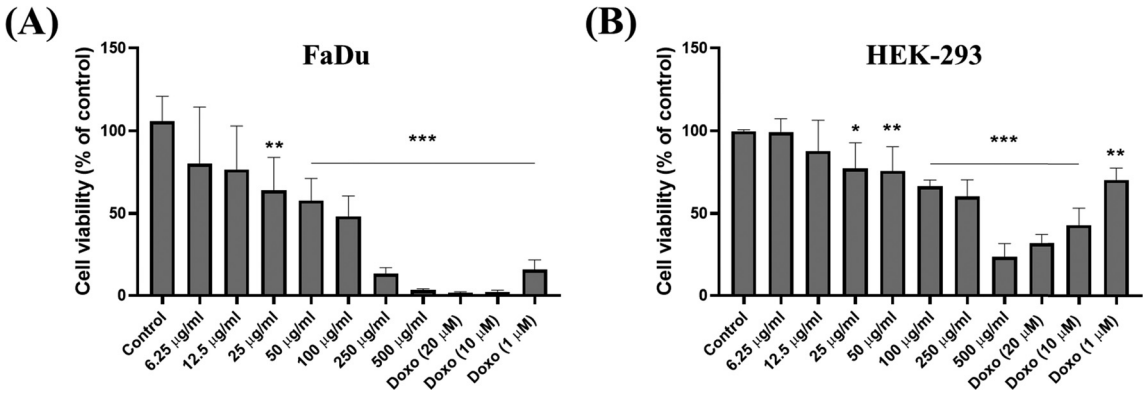

Fig. 6 Cytotoxic effect of Ti_3C_2(O,Cl) MXene on FaDu (A) and HEK-293 (B) cells for a time duration of 48 h. Data are shown as mean ± SD (n = 3) of three independent experiments. *** $p < 0.001$, ** $p < 0.01$, and * $p < 0.05$ *vs.* respective control.

cells compared to FaDu and MCF-7 cell lines over a 24-h time period, as illustrated in Fig. 5(C) and (D) for 24 h. Moreover, the observed cytotoxic effects were higher against cancerous cells in comparison to the normal ones.

Furthermore, the presence of dual oxygen (O) and chlorine (Cl) functional groups on Ti_3C_2(O,Cl) MXene appears to enhance preferential cytotoxicity toward cancer cells due to differential redox thresholds, likely due to these groups' capacity to generate localized oxidative stress or disrupt specific cancer cell processes more effectively.[41] Cancer cells, with higher metabolic rates and altered redox balances, may be more susceptible to the reactive oxygen species (ROS) or cellular disruptions triggered by these functional groups,[42] explaining the observed preference in cytotoxicity towards cancer cells over the normal ones. Moreover, selectivity was not ligand-receptor mediated but arose from cancer cells' intrinsic susceptibility to oxidative stress. Similarly, a previously reported study also compared the effects of $Ti_3C_2T_x$ nanosheets on two non-malignant cell lines (MRC-5 and HaCaT) and two cancer lines (A549 and A375), observing that the nanomaterial was markedly more toxic to the tumor cells than to healthy cells.[26] Moreover, a recent study evaluated the short-term cytotoxicity of several $Ti_3C_2T_x$ MXene variants and their carbide precursors (TiC, Ti_2AlC, and Ti_3AlC_2) and found significantly greater cell death in HeLa cancer cells than in normal human fibroblasts. These selective effects have been linked to elevated reactive oxygen species generation and stronger MXene-membrane interactions in malignant cells.[43] A recent study focused on antibacterial applications highlights that Cl-terminated Ti_3C_2 MXenes generate higher ROS compared to other functional groups (*e.g.*, –OH and –F). Combined with oxygen groups, this supports the plausibility of O/Cl synergy in cancer-selective toxicity.[44] Additionally, surface functionalization of O and –Cl of MXenes enhances their interactions with cancer cell membranes, promoting selective uptake and ROS-mediated cell death.[45]

There could be a metabolic variation among the cells that leads to this outcome. The observed differences in cytotoxicity across cell lines likely result from variations in cellular metabolism, membrane properties, and oxidative stress responses.[41,46] Cancer cells like FaDu and MCF-7 often exhibit higher metabolic activity and increased ROS production,[47] making them more susceptible to oxidative stress induced by Ti_3C_2(O,Cl) MXene. These cells may also have altered membrane characteristics that enhance the uptake of nanoparticles, leading to increased cytotoxicity. Normal cell lines such as H9C2 and HEK293 are known to possess stronger antioxidant defense systems, including higher expression of enzymes like superoxide dismutase (SOD), catalase, and glutathione peroxidase, which help mitigate ROS-mediated cytotoxicity.[48,49] In contrast, many cancer cells exhibit elevated basal ROS levels due to mitochondrial dysfunction and oncogenic signaling, making them more susceptible to additional oxidative stress-induced damage.[41] Eukaryotic cells tightly regulate ROS production and scavenging to maintain redox homeostasis. Cancer cells, however, frequently exhibit dysregulated ROS metabolism, which supports both survival and progression under oxidative stress.[50,51] MXenes, due to their surface chemistry, can exacerbate oxidative conditions selectively in tumor cells.[52,53] The increased cytotoxicity observed in FaDu cells after 48 hours may thus reflect a time-dependent accumulation of ROS that overwhelms the already stressed antioxidant systems in cancer cells. It is now recognized that ROS mediate a complex network of interactions within the tumor microenvironment, influencing stromal cells, angiogenesis, and immune responses. The therapeutic modulation of ROS, though promising, remains context-dependent and is influenced by factors such as ROS type, level, localization, and tumor stage.[50,51] Our findings suggest that dual-functionalized Ti_3C_2(O,Cl) MXenes may tip this redox balance selectively in favor of cancer cell apoptosis. As in MTT testing, the Ti_3C_2(O,Cl) MXene tested material displayed inverse proportionality between the number of living cells and concentration, as well as higher selectivity against cancerous cells. The results obtained suggest that these effects may be a consequence of differences between the morphology and the permeability of normal and cancerous cells.

3.3 Mechanisms of toxicity

Carbon-based nanomaterials have been shown to exhibit cytotoxicity due to reactive oxygen species (ROS) that play a key role

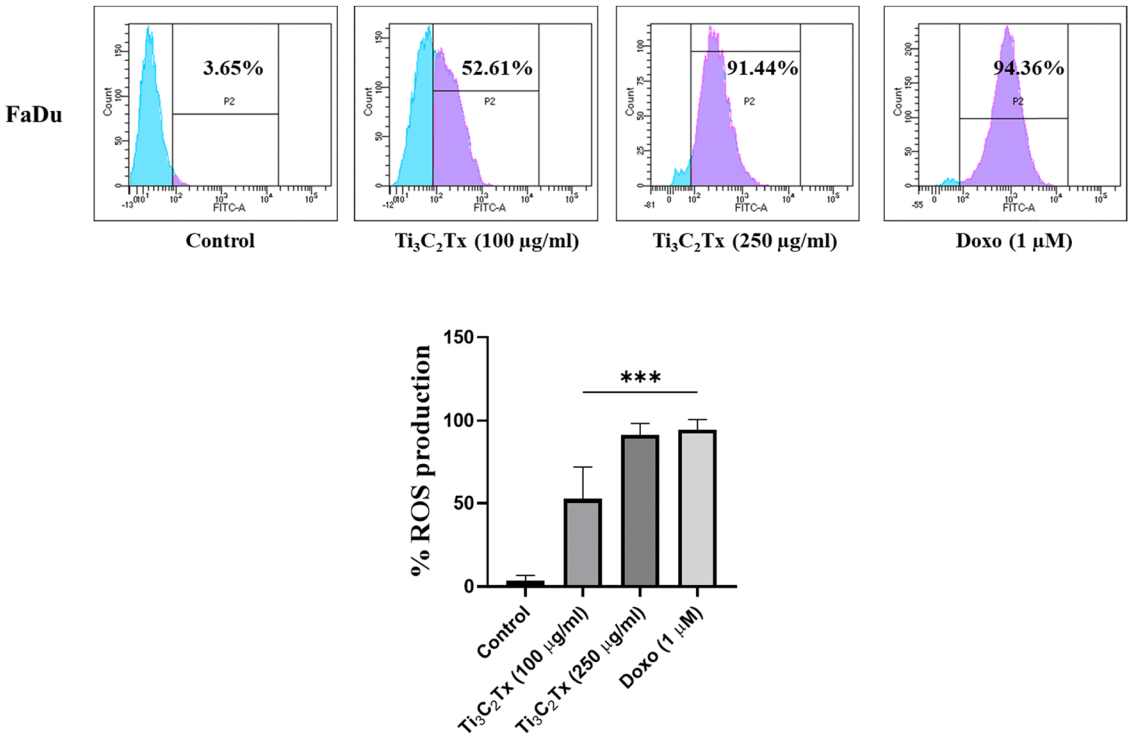

Fig. 7 $Ti_3C_2(O,Cl)$ MXene and Doxo induced reactive oxygen species (ROS) production in FaDu cells for 24 h. Data are shown as mean ± SD (n = 3) of three independent experiments. *** $p < 0.001$ *vs.* control.

in cell metabolism and survival.[54] DCF-DA assays were conducted to determine whether the decreased cell viability after $Ti_3C_2(O,Cl)$ MXene treatment is caused by oxidative stress phenomena in cancerous FaDu and normal HEK-293 cells for 24 h. As shown in Fig. 7 and 8, after 24 h of incubating MXene with 100 and 250 μg mL^{-1} and Doxo 1 μM in FaDu cells, a significant increase in ROS production (a parameter proportional to the level of intracellular reactive oxygen species) was observed as compared to control untreated cells (52.61, 91.44, and 94.36%, respectively, to 100, 250 μg mL^{-1} $Ti_3C_2(O,Cl)$ MXene and Doxo 1 μM) ($p < 0.001$; Fig. 7).

Similarly, to check the selective ROS production effect of MXene in normal HEK-293 cells, we have treated $Ti_3C_2(O,Cl)$ MXene 100 μg mL^{-1} and Doxo 1 μM in HEK-293 cells for 24 h. Interestingly, less ROS production was observed in HEK-293 cells compared to FaDu cells for 24 h, as depicted in Fig. 8. This result suggests that $Ti_3C_2(O,Cl)$ MXene has more selectivity towards cancer cells as compared to the normal cell line. The results obtained allow us to propose ROS generation as the possible mechanism of the cytotoxicity of $Ti_3C_2(O,Cl)$ MXene.

However, our results demonstrated a dose-dependent and significantly higher cytotoxicity of $Ti_3C_2(O,Cl)$ MXene in cancer cell lines FaDu and MCF-7 compared to normal cell lines H9C2 and HEK-293. This enhanced cytotoxicity in cancerous cells is likely due to differences in intracellular internalization mechanisms and ROS production between malignant and non-malignant cells. Cancer cells are known to exhibit altered membrane characteristics that facilitate greater uptake of nanoparticles, leading to a higher intracellular concentration of $Ti_3C_2(O,Cl)$ MXene, which amplifies ROS production and induces oxidative stress. Additionally, cancer cells often experience elevated baseline oxidative stress due to their metabolic demands and rapid proliferation, rendering them more vulnerable to further ROS generation upon MXene exposure. The heightened ROS levels overwhelm cancer cells' already compromised antioxidant defences, resulting in cell damage and death. In contrast, normal cells such as H9C2 and HEK-293 typically maintain stronger antioxidant defences and lower baseline ROS levels, enabling them to better neutralize the ROS induced by $Ti_3C_2(O,Cl)$ MXene. This ROS-mediated mechanism aligns with previous studies highlighting the selective cytotoxicity of MXenes toward cancer cells, supporting their potential as targeted anticancer agents.

3.4. Comparative analysis with previous MXene reports

A direct comparison with earlier MXene reports highlights the benefits of our electrochemical dual functionalization. We observe a (002) XRD peak shift from 10.627° to 10.360° ($\Delta 2\theta = 0.27°$), slightly larger than the $\Delta 2\theta = 0.22°$ shift reported for Cl terminated $Ti_3C_2Cl_x$ obtained *via* molten salt etching.[55] High resolution XPS reveals a Ti–Cl/Ti–C area ratio of 0.57, markedly higher than the ~0.35 ratio in HF etched $Ti_3C_2T_x$ samples.[56] Biologically, our IC_{50} of ≈48 μg mL^{-1} on FaDu cells (SI = 2.7) compares favorably to ≈50 μg mL^{-1} (SI ≈ 1.8) reported for Ti_3C_2 MXenes against A549 carcinoma.[57] These results confirm that the incorporation of both –O and –Cl terminations *via* chronoamperometric etching yields superior interlayer expansion, surface chemical functionality, and

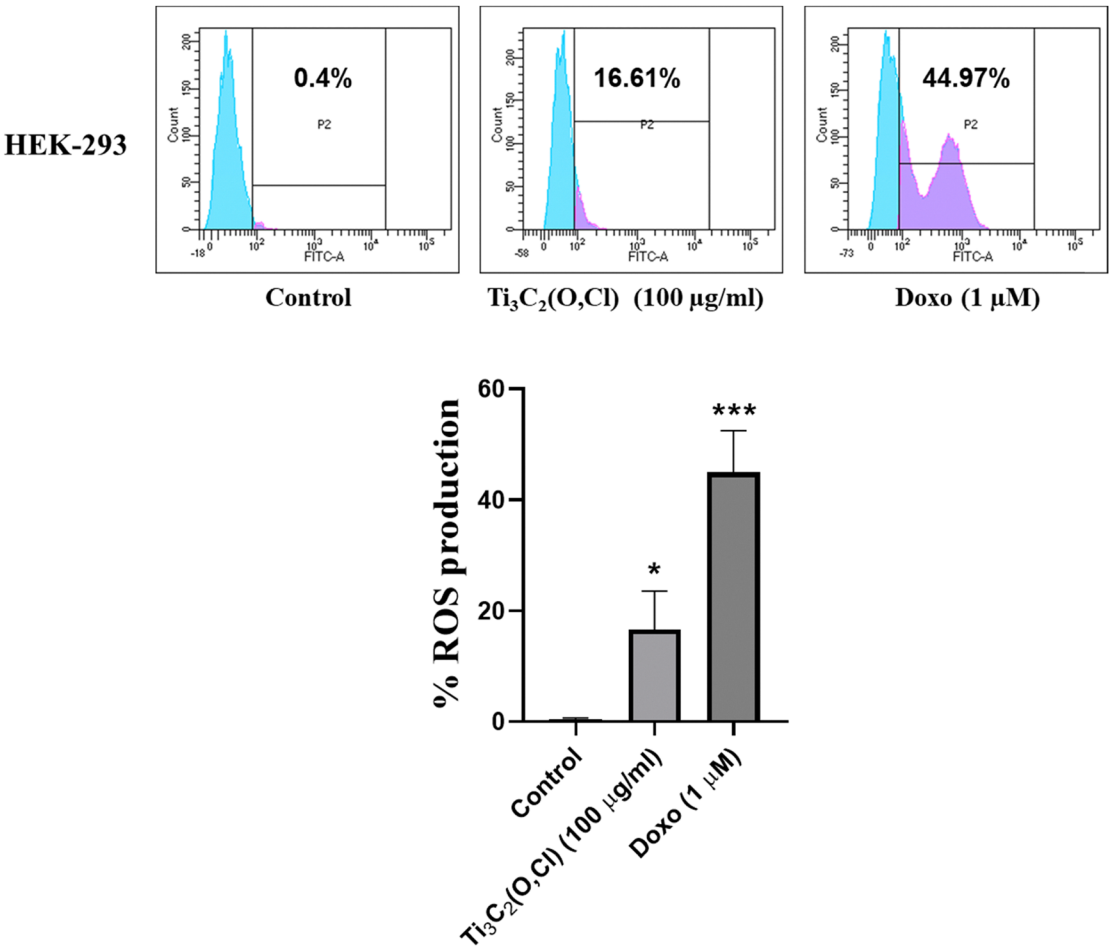

Fig. 8 MXene and Doxo induced reactive oxygen species (ROS) production in HEK-293 cells for 24 h. Data are shown as mean ± SD (n = 3) of three independent experiments. *** $p < 0.001$ and * $p < 0.05$ *vs.* control.

Table 3 Comparative metrics for $Ti_3C_2(O,Cl)$ MXene *versus* AuNPs and IONPs in anticancer activity

Nanomaterial	IC_{50} (cancer)	IC_{50} (normal)	SI (normal/cancer)	Mechanism	Ref.
$Ti_3C_2(O,Cl)$ MXene	48 µg mL^{-1} (FaDu)	130 µg mL^{-1} (HEK-293)	2.7	Dual O/Cl terminations generate localized ROS, exploiting cancer cells' heightened redox sensitivity	Present study
HA-capped AuNPs	34.8 µg mL^{-1} (MDA-MB-231)	935.97 µg mL^{-1} (L929)	26.9	Photothermal conversion plus HA-mediated CD44-targeted uptake	59
Fe_3O_4@Glu-Safranal IONPs	305 µg mL^{-1} (HepG2)	680 µg mL^{-1} (HEK-293)	2.23	Fenton reaction-driven ROS generation in the acidic tumor microenvironment	58

selective anticancer efficacy relative to conventional MXene synthesis methods.

3.5 Comparative advantages of dual-functionalized $Ti_3C_2(O,Cl)$ MXenes in targeted cancer therapy

Dual functionalized $Ti_3C_2(O,Cl)$ MXenes show strong cytotoxicity against squamous carcinoma and adenocarcinoma cells ($IC_{50} \approx 48$ µg mL^{-1}) with a selectivity index (SI) of ≈2.7, which is better than that of iron oxide nanoparticles ($IC_{50} \approx 305$ µg mL^{-1}; SI ≈ 2.2)[58] and comparable to that of hyaluronic acid-capped AuNPs ($IC_{50} \approx 34.8$ µg mL^{-1}; SI ≈ 26.9)[59] as represented in Table 3. MXenes with distinct –O/–Cl terminations catalyze localized ROS formation, taking advantage of cancer cells' higher basal oxidative stress in the absence of external stimuli, while their nearly unity photothermal conversion allows synergistic thermal ablation. In contrast, AuNPs use mainly plasmon-induced heating and receptor-mediated uptake for selectivity, and iron oxide systems rely on Fenton chemistry in acidic tumor microenvironments and magnetic targeting.[58] Additionally, the high conductivity and modifiable surface chemistry of MXenes enable loading of drugs, imaging, and multimodal therapy in a unified platform. Critically, they eschew sophisticated instrumentation demands like NIR lasers or magnetic fields, which simplifies their clinical translation and minimizes cost.

6. Conclusion

The current investigation demonstrates the successful etching of scalable synthesized Ti_3C_2(O,Cl) MXenes *via* electrochemical methods. XRD reveals that 73.7% of Ti_3C_2(O,Cl) was successfully etched from the Ti_3AlC_2 MAX phase, and the etched Ti_3C_2(O,Cl) MXenes exhibit a consistent structure, as agreed by TEM and SEM analyses. Raman and XPS analyses, along with FTIR, reveal that the surface terminations on Ti_3C_2 MXenes include –O, –Cl, and –OH. These surface terminations suggest a strengthened cytotoxic effect on cancer cells. This investigation elucidated multiple facets of the *in vitro* cytotoxicity of Ti_3C_2(O,Cl) MXene in relation to both cancerous and normal cells, confirming a notable toxicity level of approximately 91% against cancer cells. Moreover, the phenomena associated with oxidative stress are recognized as possible mechanisms of toxicity in our investigation. MXenes have demonstrated toxicity towards anticancer cells; the present study offers the latest insights into these compounds. Concerns regarding toxicity have impeded further research and development in the realms of nanomedicine and targeted cancer therapies.

Data availability

Data generated at BITS Pilani Hyderabad Campus are available upon request. Experiments were conducted at BITS Pilani Hyderabad Campus. Experimental data supporting the findings of this study are available from the corresponding author, Prof Afkham Mir (mirafkham@hyderabad.bits-pilani.ac.in), on request.

Conflicts of interest

There are no conflicts to declare.

Acknowledgements

This work was supported by the SPARKLE grant from BITS Pilani, Hyderabad Campus.

References

1 M. J. Thun, J. O. DeLancey, M. M. Center, A. Jemal and E. M. Ward, The global burden of cancer: priorities for prevention, *Carcinogenesis*, 2010, **31**, 100–110.
2 C. Mattiuzzi and G. Lippi, Current cancer epidemiology, *J. Epidemiol. Global Health*, 2019, **9**, 217–222.
3 B. Liu, H. Zhou, L. Tan, K. T. H. Siu and X.-Y. Guan, Exploring treatment options in cancer: tumor treatment strategies, *Signal Transduction Targeted Ther.*, 2024, **9**, 175.
4 A. H. Alkhathlan, H. A. Al-Abdulkarim, M. Khan, M. Khan, M. Alkholief, A. Alshamsan, A. Almomen, N. Albekairi, H. Z. Alkhathlan and M. R. H. Siddiqui, Evaluation of the anticancer activity of phytomolecules conjugated gold nanoparticles synthesized by aqueous extracts of Zingiber officinale (ginger) and Nigella sativa L. seeds (black cumin), *Materials*, 2021, **14**, 3368.
5 Q. Yin, L. Tan, Q. Lang, X. Ke, L. Bai, K. Guo, R. Qiao and S. Bai, Plasmonic molybdenum oxide nanosheets supported silver nanocubes for enhanced near-infrared antibacterial activity: Synergism of photothermal effect, silver release and photocatalytic reactions, *Appl. Catal., B*, 2018, **224**, 671–680.
6 D. Krzyzanowski, M. Kruszewski and A. Grzelak, Differential action of silver nanoparticles on ABCB1 (MDR1) and ABCC1 (MRP1) activity in mammalian cell lines, *Materials*, 2021, **14**, 3383.
7 S. J. Zhen, T. T. Wang, Y. X. Liu, Z. L. Wu, H. Y. Zou and C. Z. Huang, Reduced graphene oxide coated $Cu_{2-x}Se$ nanoparticles for targeted chemo-photothermal therapy, *J. Photochem. Photobiol., B*, 2018, **180**, 9–16.
8 W. Wei, X. Zhang, S. Zhang, G. Wei and Z. Su, Biomedical and bioactive engineered nanomaterials for targeted tumor photothermal therapy: A review, *Mater. Sci. Eng., C*, 2019, **104**, 109891.
9 B. Guo, J. Zhao, C. Wu, Y. Zheng, C. Ye, M. Huang and S. Wang, One-pot synthesis of polypyrrole nanoparticles with tunable photothermal conversion and drug loading capacity, *Colloids Surf., B*, 2019, **177**, 346–355.
10 S. Yang, L. Zhou, Y. Su, R. Zhang and C.-M. Dong, One-pot photoreduction to prepare NIR-absorbing plasmonic gold nanoparticles tethered by amphiphilic polypeptide copolymer for synergistic photothermal-chemotherapy, *Chin. Chem. Lett.*, 2019, **30**, 187–191.
11 M. Naguib, M. Kurtoglu, V. Presser, J. Lu, J. Niu, M. Heon, L. Hultman, Y. Gogotsi and M. W. Barsoum, Two-dimensional nanocrystals produced by exfoliation of Ti_3AlC_2, *Adv. Mater.*, 2011, **23**, 4248–4253.
12 M. Ghidiu, M. R. Lukatskaya, M.-Q. Zhao, Y. Gogotsi and M. W. Barsoum, Conductive two-dimensional titanium carbide 'clay'with high volumetric capacitance, *Nature*, 2014, **516**, 78–81.
13 J. Pang, R. G. Mendes, A. Bachmatiuk, L. Zhao, H. Q. Ta, T. Gemming, H. Liu, Z. Liu and M. H. Rummeli, Applications of 2D MXenes in energy conversion and storage systems, *Chem. Soc. Rev.*, 2019, **48**, 72–133.
14 M. Hu, C. Cui, C. Shi, Z.-S. Wu, J. Yang, R. Cheng, T. Guang, H. Wang, H. Lu and X. Wang, High-energy-density hydrogen-ion-rocking-chair hybrid supercapacitors based on $Ti_3C_2T_x$ MXene and carbon nanotubes mediated by redox active molecule, *ACS Nano*, 2019, **13**, 6899–6905.
15 M. Naguib; M. Kurtoglu; V. Presser; J. Lu; J. Niu; M. Heon; L. Hultman; Y. Gogotsi and M. W. Barsoum, Two-dimensional nanocrystals produced by exfoliation of Ti_3AlC_2, in *Mxenes*, Jenny Stanford Publishing, 2023, pp. 15–29.
16 A. Gentile, S. Marchionna, M. Balordi, G. Pagot, C. Ferrara, V. Di Noto and R. Ruffo, Critical analysis of MXene production with *in situ* HF forming agents for sustainable manufacturing, *ChemElectroChem*, 2022, **9**, e202200891.
17 Y. Li, H. Shao, Z. Lin, J. Lu, L. Liu, B. Duployer, P. O. Persson, P. Eklund, L. Hultman and M. Li, A general Lewis acidic etching route for preparing MXenes with enhanced

electrochemical performance in non-aqueous electrolyte, *Nat. Mater.*, 2020, **19**, 894–899.

18 B. C. Wyatt, M. G. Boebinger, Z. D. Hood, S. Adhikari, P. P. Michałowski, S. K. Nemani, M. G. Muraleedharan, A. Bedford, W. J. Highland and P. R. Kent, Alkali cation stabilization of defects in 2D MXenes at ambient and elevated temperatures, *Nat. Commun.*, 2024, **15**, 6353.

19 J. Yang, M. Naguib, M. Ghidiu, L. M. Pan, J. Gu, J. Nanda, J. Halim, Y. Gogotsi and M. W. Barsoum, Two-dimensional Nb-based M4C3 solid solutions (MXenes), *J. Am. Ceram. Soc.*, 2016, **99**, 660–666.

20 C. Peng, P. Wei, X. Chen, Y. Zhang, F. Zhu, Y. Cao, H. Wang, H. Yu and F. Peng, A hydrothermal etching route to synthesis of 2D MXene (Ti_3C_2, Nb_2C): Enhanced exfoliation and improved adsorption performance, *Ceram. Int.*, 2018, **44**, 18886–18893.

21 S. Tian, G. Cheng, Z. Tang, F. Sha, Z. Xuan and G. Ding, Fabrication of two-dimensional $Ti_3C_2T_x$ MXenes by ball milling pretreatment and mild etchant and their microstructure, *Ceram. Int.*, 2020, **46**, 28949–28954.

22 Z. Abid, K. Rafiq, A. Aslam, R. Jin and E. Hussain, Scope, evaluation and current perspectives of MXene synthesis strategies for state of the art applications, *J. Mater. Chem. A*, 2024, **12**, 7351–7395.

23 M. Zhao, C. Casiraghi and K. Parvez, Electrochemical exfoliation of 2D materials beyond graphene, *Chem. Soc. Rev.*, 2024, **53**, 3036–3064.

24 S. Yang, P. Zhang, F. Wang, A. G. Ricciardulli, M. R. Lohe, P. W. Blom and X. Feng, Fluoride-free synthesis of two-dimensional titanium carbide (MXene) using a binary aqueous system, *Angew. Chem.*, 2018, **130**, 15717–15721.

25 L. Liu, H. Zschiesche, M. Antonietti, M. Gibilaro, P. Chamelot, L. Massot, P. Rozier, Pl Taberna and P. Simon, *In situ* synthesis of MXene with tunable morphology by electrochemical etching of MAX phase prepared in molten salt, *Adv. Energy Mater.*, 2023, **13**, 2203805.

26 A. Jastrzębska, A. Szuplewska, T. Wojciechowski, M. Chudy, W. Ziemkowska, L. Chlubny, A. Rozmysłowska and A. Olszyna, In vitro studies on cytotoxicity of delaminated Ti_3C_2 MXene, *J. Hazard. Mater.*, 2017, **339**, 1–8.

27 A. Jastrzębska, A. Szuplewska, A. Rozmysłowska-Wojciechowska, M. Chudy, A. Olszyna, M. Birowska, M. Popielski, J. Majewski, B. Scheibe and V. Natu, On tuning the cytotoxicity of Ti_3C_2 (MXene) flakes to cancerous and benign cells by post-delamination surface modifications, *2D Mater.*, 2020, **7**, 025018.

28 A. Fernando and J. Gariépy, Coupling Chlorin e6 to the surface of Nanoscale Gas Vesicles strongly enhances their intracellular delivery and photodynamic killing of cancer cells, *Sci. Rep.*, 2020, **10**, 2802.

29 S. Z. Yıldız, C. Bilir, G. G. Eskiler and F. Bilir, The anticancer potential of chlorine dioxide in small-cell lung cancer cells, *Cureus*, 2022, 14.

30 B. Rashid; N. Sridewi; A. Anwar; S. Shahabbudin and A. A. Mon, A review on human cancer and potential role of MXenes in cancer therapy, in *Proceedings of the E3S Web of Conferences*, 2024, p. 03021.

31 G. Liu, J. Zou, Q. Tang, X. Yang, Y. Zhang, Q. Zhang, W. Huang, P. Chen, J. Shao and X. Dong, Surface modified Ti_3C_2 MXene nanosheets for tumor targeting photothermal/photodynamic/chemo synergistic therapy, *ACS Appl. Mater. Interfaces*, 2017, **9**, 40077–40086.

32 Z. Wang, Z. Run, H. Wang, X. He and J. Li, TiO_2–Ti_3C_2 Nanocomposites Utilize Their Photothermal Activity for Targeted Treatment of Colorectal Cancer, *Int. J. Nanomed.*, 2024, 1041–1054.

33 L. Chen, Y. Cao, X. Zhang, X. Guo, P. Song, K. Chen and J. Lin, Anisotropic and high thermal conductivity of epoxy composites containing multilayer $Ti_3C_2T_x$ MXene nanoflakes, *J. Mater. Sci.*, 2020, **55**, 16533–16543.

34 W. Sun, S. Shah, Y. Chen, Z. Tan, H. Gao, T. Habib, M. Radovic and M. Green, Electrochemical etching of Ti_2AlC to Ti_2CT_x (MXene) in low-concentration hydrochloric acid solution, *J. Mater. Chem. A*, 2017, **5**, 21663–21668.

35 Y. Cao, C. Guo and Y. Zou, Rapid synthesis of MXenes at room temperature, *Mater. Sci. Technol.*, 2019, **35**, 1904–1907.

36 O. Mashtalir, *Chemistry of two-dimensional transition metal carbides (MXenes)*, Drexel University, 2015.

37 A. Sarycheva and Y. Gogotsi, Raman spectroscopy analysis of the structure and surface chemistry of $Ti_3C_2T_x$ Mxene, in *Mxenes*, Jenny Stanford Publishing, 2023, pp. 333–355.

38 S. Kumar, M. A. Rehman, S. Lee, M. Kim, H. Hong, J.-Y. Park and Y. Seo, Supercapacitors based on $Ti_3C_2T_x$ MXene extracted from supernatant and current collectors passivated by CVD-graphene, *Sci. Rep.*, 2021, **11**, 649.

39 A. Al Mayyahi, S. Sarker, B. M. Everhart, B. Tonyali, U. Yucel and P. B. Amama, Synthesis of ultrathin, nano-sized $Ti_3C_2T_x$ with abundant =O and –OH terminals and high transparency as a cocatalyst: Enabling design of high-performance Titania-$Ti_3C_2T_x$ hybrid photocatalysts, *J. Phys. Chem. Solids*, 2022, **170**, 110875.

40 A. Mateen, M. Z. Ansari, Q. Abbas, A. Muneeb, A. Hussain, E. T. Eldin, F. M. Alzahrani, N. S. Alsaiari, S. Ali and M. S. Javed, *In situ* nitrogen functionalization of 2D-$Ti_3C_2T_x$-MXenes for high-performance Zn-ion supercapacitor, *Molecules*, 2022, **27**, 7446.

41 D. Trachootham, J. Alexandre and P. Huang, Targeting cancer cells by ROS-mediated mechanisms: a radical therapeutic approach?, *Nat. Rev. Drug Discovery*, 2009, **8**, 579–591.

42 C. Gorrini, I. S. Harris and T. W. Mak, Modulation of oxidative stress as an anticancer strategy, *Nat. Rev. Drug Discovery*, 2013, **12**, 931–947.

43 Be Scheibe, J. K. Wychowaniec, M. Scheibe, B. Peplińska, M. Jarek, G. Nowaczyk and Ł. Przysiecka, Cytotoxicity assessment of Ti–Al–C based MAX phases and $Ti_3C_2T_x$ MXenes on human fibroblasts and cervical cancer cells, *ACS Biomater. Sci. Eng.*, 2019, **5**, 6557–6569.

44 Y. Xu, H. Zhang, Y. Jing, X. Wang, J. Gan, Z. Yan, X. Liu, J. Wu and Z. Lan, Cl-terminated Ti_3C_2 MXene-modulated carbon/CsPbIBr2 interface boosting efficiency and stability of all-inorganic perovskite solar cells, *Appl. Surf. Sci.*, 2023, **619**, 156674.

45 S. Iravani and R. S. Varma, MXenes for cancer therapy and diagnosis: recent advances and current challenges, *ACS Biomater. Sci. Eng.*, 2021, **7**, 1900–1913.
46 G.-Y. Liou and P. Storz, Reactive oxygen species in cancer, *Free Radical Res.*, 2010, **44**, 479–496.
47 I. Ullah, A. T. Khalil, M. Ali, J. Iqbal, W. Ali, S. Alarifi and Z. K. Shinwari, Green-synthesized silver nanoparticles induced apoptotic cell death in MCF-7 breast cancer cells by generating reactive oxygen species and activating caspase 3 and 9 enzyme activities, *Oxid. Med. Cell. Longevity*, 2020, **2020**, 1215395.
48 H. Nakamura and K. Takada, Reactive oxygen species in cancer: Current findings and future directions, *Cancer Sci.*, 2021, **112**, 3945–3952.
49 B. Fernández-Rojas, G. I. Vázquez-Cervantes, J. Pedraza-Chaverri and G. Gutiérrez-Venegas, Lipoteichoic acid reduces antioxidant enzymes in H9c2 cells, *Toxicol. Rep.*, 2020, **7**, 101–108.
50 C. R. Reczek and N. S. Chandel, The two faces of reactive oxygen species in cancer, *Annu. Rev. Cancer Biol.*, 2017, **1**, 79–98.
51 J. N. Moloney and T. G. Cotter, ROS signalling in the biology of cancer, in *Proceedings of the Seminars in cell & developmental biology*, 2018, pp. 50–64.
52 T. Malina, B. Hamawandi, M. S. Toprak, L. Chen, J. Björk, J. Zhou, J. Rosen and B. Fadeel, Tuning the transformation and cellular signaling of 2D titanium carbide MXenes using a natural antioxidant, *Matter*, 2024, **7**, 191–215.
53 T. Li, W. Qiang and B. Lei, Bioactive surface functionalized MXenes for Biomedicine, *Nanoscale*, 2025, **17**, 4854–4891.
54 W. Hu, C. Peng, W. Luo, M. Lv, X. Li, D. Li, Q. Huang and C. Fan, Graphene-based antibacterial paper, *ACS Nano*, 2010, **4**, 4317–4323.
55 D. D. Kruger, H. García and A. Primo, Molten Salt Derived MXenes: Synthesis and Applications, *Adv. Sci.*, 2024, **11**, 2307106.
56 L.-Å. Näslund, P. O. Persson and J. Rosen, X-ray photoelectron spectroscopy of Ti3AlC2, $Ti_3C_2T_z$, and TiC provides evidence for the electrostatic interaction between laminated layers in MAX-phase materials, *J. Phys. Chem. C*, 2020, **124**, 27732–27742.
57 B. Rashid, A. Anwar, S. Shahabuddin, G. Mohan, R. Saidur, N. Aslfattahi and N. Sridewi, A comparative study of cytotoxicity of PPG and PEG Surface-Modified 2-D Ti_3C_2 MXene Flakes on Human Cancer cells and their Photothermal response, *Materials*, 2021, **14**, 4370.
58 S. Mikaeili Ghezeljeh, A. Salehzadeh and S. Ataei-e Jaliseh, Iron oxide nanoparticles coated with Glucose and conjugated with Safranal (Fe_3O_4@ Glu-Safranal NPs) inducing apoptosis in liver cancer cell line (HepG2), *BMC Chem.*, 2024, **18**, 33.
59 J. Wang, N. Liu, Q. Su, Y. Lv, C. Yang and H. Zhan, Green synthesis of gold nanoparticles and study of their inhibitory effect on bulk cancer cells and cancer stem cells in breast carcinoma, *Nanomaterials*, 2022, **12**, 3324.